ANNEXURE

SYNTHESIS, STRUCTURAL AND ELECTRICAL CHARACTERIZATIONS OF GRAPHENE OXIDE – HYDROXYAPATITE NANOCOMPOSITES

A.1 Introduction

Carbon based nanomaterials have been used in wide range of applications. Their performance originates largely from controlling the structural polymorphism and chemical stability, this including size, length, chirality and the number of layers. Variations in synthesis technique, temperature, pressure, catalyst, electron field optimize nanomaterial structure, purity and physical orientation for specific applications [1]. Micro-structured carbon materials, such as carbon nanotubes (CNT), improve electrochemical applications by enabling novel designs in sensing, electro catalysis and electronics, compared to traditional carbon materials such as glassy carbon, diamond or carbon black. Most recently, graphene oxide (GO) emerged as a material with future potential for improved applications. These expectations are based on the more advanced properties of GO compared to CNTs [2].

Graphene oxide is a two dimensional monolayer of sp^2 carbon in a honeycomb-like network. It has attracted a great deal of scientific interest due to its outstanding mechanical, electrical, thermal, and optical properties [3-6]. The outstanding properties of GO depend on the number of layers and its dispersion. Due to Van der Waals and π-π stacking interactions among individual GO sheets, they have a tendency to aggregate when GO dispersion solutions are dried. Incorporation of nanomaterials into GO sheets prevents them from becoming agglomerated and also helps in achieving a good distribution of NPs. Thus, the effective surface area available for the gas interaction increases by several times [7]. So that GO based nanocomposites show improved property than the NPs or GO. Large number of

research publications based on nanocomposites of graphene with metal [8-12], metal oxide [13-18] and semiconductor quantum dots [19, 20] have been reported.

Hydroxyapatite crystallizes in a hexagonal crystal structure is the primary chemical constituent of bone and teeth and it has been extensively evaluated for its biocompatibility. It has been utilized in the medical field. Additionally, HAP has interesting chemical property, such as adsorption and separation of nucleic acids and dehydration and dehydration of alcohols, oxidation catalyst, and thus may be employed as a chemical sensor or in electrochemical cells [21-24]. The electrical resistance of most ceramics tends to rise with irreversible adsorption of OH radicals, which increases with exposure to humidity. Since HAP contains OH radicals in its chemical makeup, it is less likely to be influenced by the presence of OH radicals. Nanostructure HAP particles with a higher surface area-to-volume-ratio would be more desirable than bulk HAP particles for their application in many fields. For example, some studies have demonstrated that HAP NPs can be used for the preparation of gas sensors [25-27], and immobilization of enzymes [28]. However, the tendency to aggregation of pure HAP-based materials limits their further applications, so it is necessary to disperse such nanomaterials in a suitable matrix to prevent aggregation. We can exploit the maximum surface property of GO and nanoscale effect of the HAP NPs by disperse the HAP in the graphene oxide layers and also this composite can exhibit a good biocompatibility. In this paper, we describe the structural and electrical studies of GO- HAP nanorods composites by XRD, TEM, UV-Vis, Raman spectroscopy and dc- conductivity.

A.2 Experimental Method

Graphite flakes (analytical grade) were oxidized using the previously reported improved Hummers method [29].

For the improved synthesis method of graphene oxide (GO), a 9:1 mixture of concentrated H_2SO_4/H_3PO_4 (360:40 ml) was added to a mixture of graphite flakes (3.0 g, 1 wt equiv) and $KMnO_4$ (18.0 g, 6 wt equiv), producing a slight exothermic about 40°C. The reaction was then heated to 50°C and stirred for 12h. The reaction was cooled to room temperature and poured onto ice (400 ml) with 30% H_2O_2 (5 ml). The resulting solid was then centrifuged and washed with 5% HCl until the supernatant was free from sulfate ions. The GO thus obtained was further washed thoroughly with double distilled water (DDW). A colloidal suspension of GO was prepared by dispersing it in 300ml DDW by sonication. This colloid solution was separated by two equal parts for further use. For the synthesis of GO-HAP composite, one part of the colloidal solution of GO (150ml) was sonicated for 10 minutes before use. After that, 100 ml of $Ca(OH)_2$ (Merck) (38.08 mM) and H_3PO_4 (CDH) (23.8 mM) solutions whose pH were adjusted to 11 were added drop wise separately to the colloidal GO solution with vigorous stirring for 2h. The resulting black solution was aged overnight without stirring. The obtained precipitate was centrifuged repeatedly with double distilled water for several times.

Thermo gravimetric analyses (TGA) were carried out using a SII Nanotechnology Inc., Japan, EXSTAR6200 thermal analyser from 35 ºC to 1000 ºC at a heating rate of 10 $^{\circ}C\ min^{-1}$ in air. The phase purity and crystal structure of the synthesised samples were analysed by powder X-ray diffractometer (Rigaku Miniflex-II) at room temperature. The scanning electron micrograph (SEM) of the samples under investigation are taken by a FEI Quanta 200 scanning electron microscope equipped

with energy dispersive analysis (EDS).TEM images were obtained using a TECHNAIG^2 TF20ST transmission electron microscope operating at 200KV. Samples for TEM were prepared by placing a drop of a colloidal acetone solution of the powder sample onto a carbon coated copper grid; the grid was dried in air. Raman spectrum of the sample was obtained at an excitation wavelength of 488 nm using a Lab-RAM HR 800 (Jobin Yvon) Raman spectrometer. The UV-visible absorption spectrum of CSNPs was measured using UV-visible spectrophotometer (Shimadzu UV-2401). The dc-conductivity of the material is characterised Keithley 236 Source Measure Unit in the temperature range from 300K to 473K. The electrical study was carried out by the GO–HAP pellet placed between the gold electrodes that whole set up were kept vacuum by using rotary pump.

A.3 Results and Discussion

A.3.1 Thermal Analysis

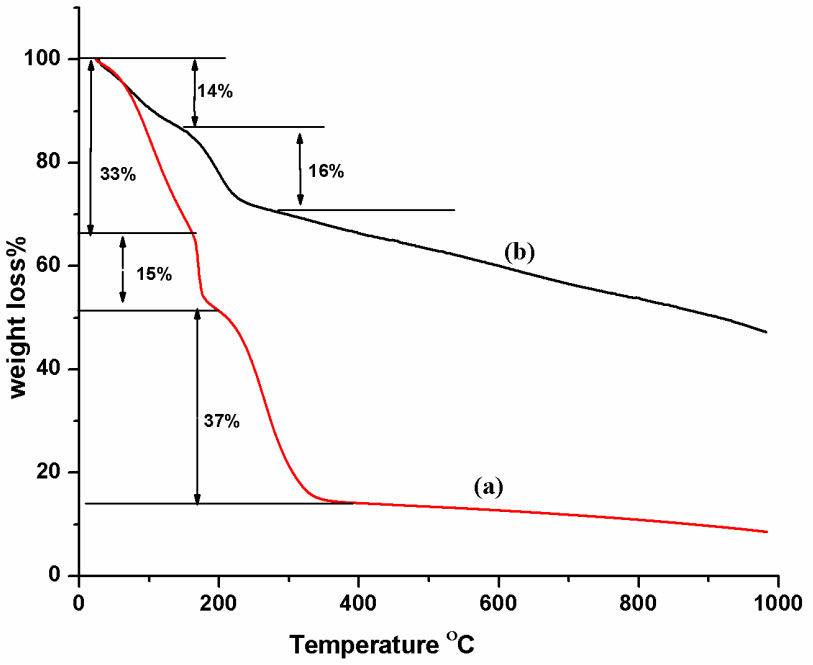

Figure A.1 Thermal analysis of (a) GO and (b) GO-HAP nanocomposite

Figure A.1 shows the thermo gravimetric study of the GO (Figure A.1a) and GO-HAP nanocomposites (Figure A.1b). From the studies, it is evident that the thermal degradation process of GO and GO-HAP nanocomposite occurs in three and two weight loss steps respectively. This indicates that GO-HAP has improved thermal stability. The GO-HAP has a lower water content (14 wt %) and it was partially converted to the reduced graphene oxide during the preparation (addition of ammonium hydroxide). Graphene oxide is thermally unstable and starts to lose mass upon heating 200 ºC, the major mass loss occurs between 200-380 ºC, presumably due to decomposition of the unstable oxygen-containing functional groups (Figure A.1a). On the other hand, the removal of the thermally labile oxygen functional groups by chemical reduction results in much increased thermal stability for the reduced GO. Apart from a slight mass loss between 160-200 ºC, which can be attributed to the loss of chemically attached functional groups, no significant mass loss is detected when this material is heated above 380^0C. For the GO-HAP nanocomposites, the first 14% mass loss (approx 180 ºC) it is due to water solvent molecules presence on the GO sheets (Figure A.1b), the following 16% decrease (270 ºC) stands for elimination of functional groups, further decomposition take place up to 800 ºC.

A.3.2 X-ray Diffraction

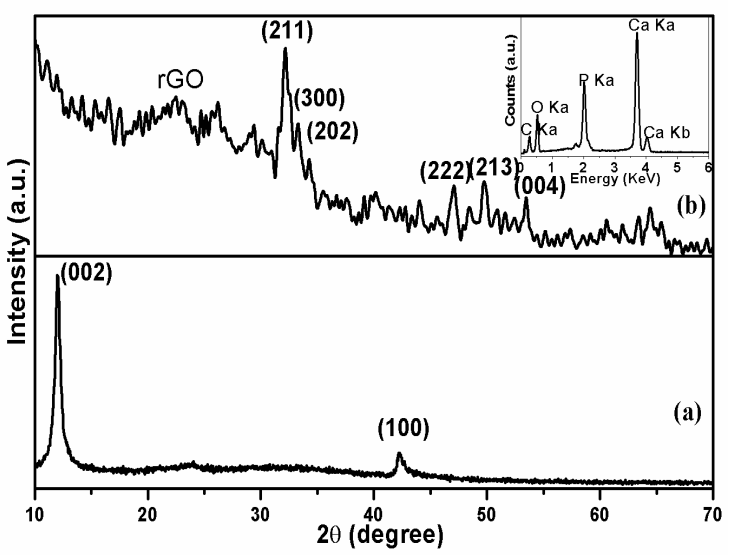

Figure A.2 X-ray diffraction patterns of (a) GO, (b) GO-HAP composites and inset Figure A.2b shows the EDS spectrum of GO-HAP nanocomposite

Figure A.2 shows XRD patterns of graphene oxide (A.2a) and GO-HAP (A.2b). In Figure A.2a, the characteristic diffraction peak (002) of GO at around 11.64°, corresponding to a d-spacing of 0.784 nm. In contrast, the interlayer distance of the (002) peak for graphite powder is 0.337 nm (2θ = 26.3°) [30]. This could be ascribed to the introduction of oxygenated functional groups, such as epoxy, hydroxyl(–OH), carboxyl (–COOH) and carbonyl (–C=O) groups attached on both sides and edges of carbon sheets. These surface functional groups will subsequently act as anchoring sites for NPs [31]. The diffraction peak at around 42.25°is associated with the (100) plane of the hexagonal structure of carbon [32].

X-ray diffraction of HAP-GO as displayed in Figure A.2b, it is obvious that the position of the strong diffraction peaks at 25.9° is attributed to the plane (002) of reduced graphene oxide. The characteristic diffraction peaks positioned at 31.8^{0}, 32.9°, 34.1° and 46.78°could be corresponding to the (211), (300), (202) and (222) crystalline planes of the HAP [24] with hexagonal phase (JCDS 89–6440)

respectively. To further confirm it is HAP loaded on the GO sheets, we undertook the energy-disperse X-ray spectrum (EDS) measurement (inset Figure A.2b) on the carbon tape. The results further reveal that the samples contain elements of calcium, phosphorous, hydrogen, carbon and oxygen.

A.3.3 Microscopic Studies

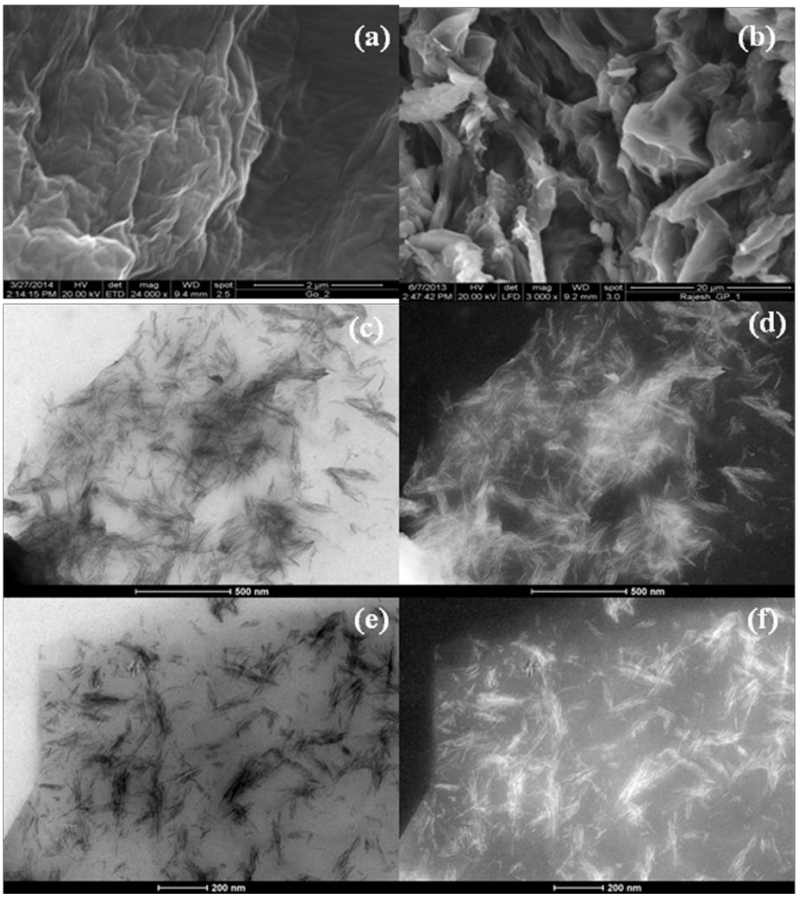

Figure A.3 SEM images of (a) GO and (b) GO-HAP nanocomposites, **Figure A.3** (c) and (e) are bright field images of GO-HAP nanocomposites and the Figure A.3 (d) and (f) are its corresponding dark field images

Scanning electron micrographs (SEM) of GO and GO-HAP nanocomposites are compared in Figures A.3a and A.3b. Layer-structured GO are stacked together and shows nearly smooth surface (Figure A.3a), while GO-HAP exhibits a number of wrinkles (Figure A.3b) and nanoscale textures, indicative of a much rougher surface.

The thin layer of graphene oxide film form is retained by nano-HAP filled on the GO layers, indicating a good interaction between nano-HAP and GO film. The morphology and size of the GO-HAP hybrids are further confirmed by TEM. Figures A.3c and A.3e shows the bright field images of GO-HAP nanocomposites and the Figures A.3d and A.3f are corresponding dark field images respectively. From this image, HAP formed in the GO layer as a rod like structure with their size is around 200 nm length and 30 nm width. To distinguish the GO and the carbon–supported film on the copper grid, dark field images of these composites are taken (Figure A.3d, A.3f), and it reveals that the high electron density HAP rods showing as white portions and the white "fog" like part is GO. Obviously, all the HAP is well mixed in the GO that no white portion is in the black area of Figure A.3d and A.3f.

A.3.4 Raman Analysis

As shown in Figure A.4a, the Raman spectrum of GO displays two prominent peaks at 1345 cm^{-1} and 1574 cm^{-1} which correspond to the well documented D and G bands respectively. The D band is ascribed to structural defects while G band is the first-order scattering of the E_{2g} vibration mode in graphene oxide sheets [33]. The spectrum of GO-HAP composites shows (Figure A.4b) with an increased intensity ratio between the D and G band (I_D/I_G) compared with that of GO [34]. It is due to the functional groups in GO sheets slightly removed and the conjugated graphene network may be established by reduction process. The established graphene network usually has a smaller average size than the original GO which will lead to a consequent increase in the intensity ratio of I_D/I_G [35]. Thus, this change of I_D/I_G suggests that graphene domains were slightly formed on GO sheets by removal of oxygen functional groups from the GO layer during the synthesis process.

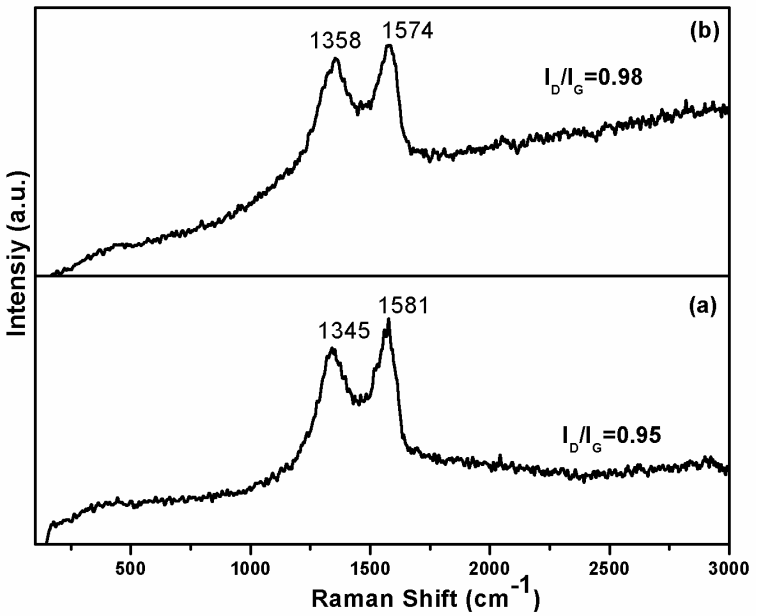

Figure A.4 Raman spectrum of (a) GO and (b) GO-HAP nanocomposite

A.3.5 UV-Visible Analysis

The as-synthesised GO exhibits optical absorption in the visible and near-infrared range (Figure A.5a). The maximum absorption peak at about 230 nm was corresponding to π-π* transition of aromatic C-C bonds [36]. Whereas a minor peak at ~318 nm attribute to n–π* transitions of C=O [37]. For the GO-HAP nanocomposites the maximum absorption peak obtained at 228 nm (Figure A.5b). The obtained optical band gap energy for GO and GO-HAP nanocomposites are found to be 4.2 and 3.5eV respectively (inset Figure A.5).

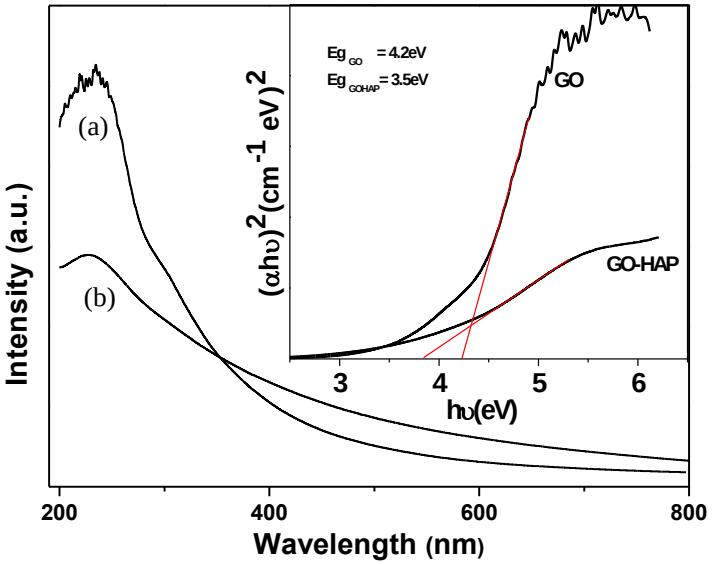

Figure A.5 UV-Visible absorbance spectra of (a) GO and (b) GO-HAP nanocomposite. Inset figure shows the plot between $(\alpha h\nu)^2$ Vs hν graph for the GO and GO-HAP nanocomposite

A.3.6 Electrical Studies

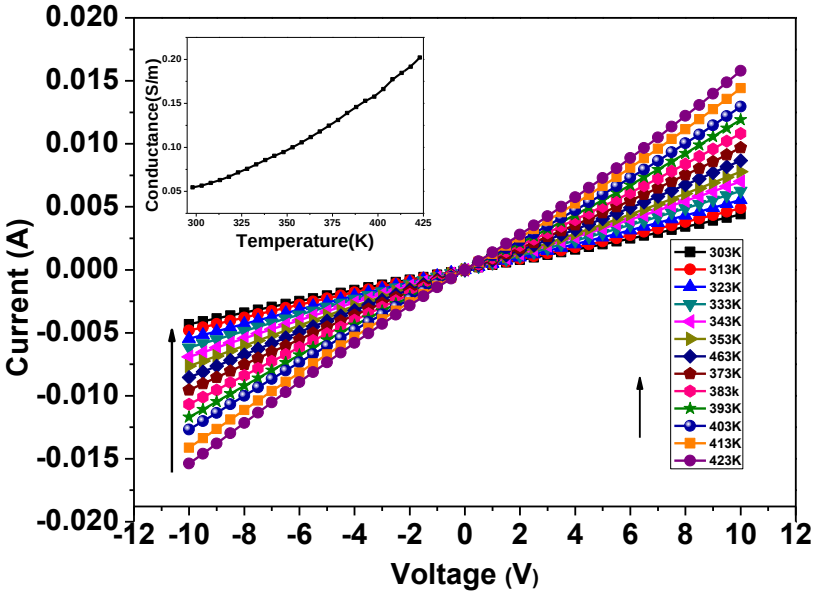

Figure A.6 Temperature-dependent I-V characteristics of the GO–HAP nanocomposites measured in the range of 300 K - 473 K and inset figure shows the temperature versus conductivity graph for GO–HAP nanocomposites

For the dc conductivity studies, GO-HAP nanocomposites were thermally reduced at 200 °C for 60 minutes. The dc-conductivity studies of this composite measured in the voltage range between -10V to 10V. The temperature-dependent I-V characteristics of the GO–HAP nanocomposites measured in the range of 300 - 473 K (FigureA.6), the graph showing nonlinear and slightly asymmetric nature, when the temperature is increasing the nonlinearity is decreasing. The nonlinearity decreases as the removal of adsorbed moisture presence the sample. Saturation of the current was not observed instead the sample resistance decreased gradually at increased dc bias.

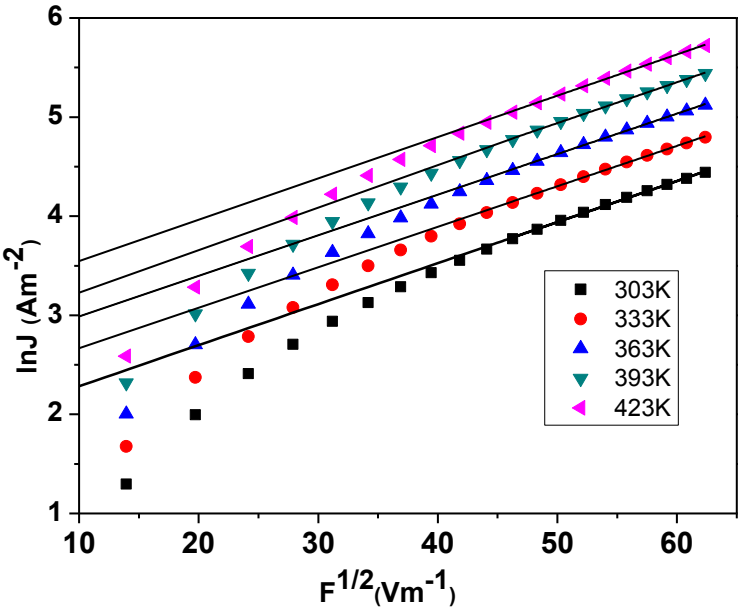

Figure A.7 Plot between lnJ and $F^{1/2}$ for I-V data in the high field region

Temperature versus conductivity graph for the pelletized GO–HAP nanocomposites is shown inset Figure A.6. The conductivity was increased with temperature almost linearly and their values beyond 300 K–426 K range from 0.05-0.20S/m. The conductivity increase as the temperature increases indicating a semiconducting behaviour [38, 39]. The conductivity value of this thermally reduced GO–HAP composite is slightly higher than the reported bare reduced graphene oxide

[40, 41] indicating that HAP nanorod has a positive effect on conduction. In graphene oxide, small cluster of sp^2 sites are separated by an amorphous and highly disordered sp^3 bonded sites, which forms a high tunnel barrier between the clusters. Resistance is decreasing while increasing the temperature associated with the formation of the cluster of touching conductive region in the graphene oxide. That is, the localized states are randomly dispersed throughout the graphene oxide [42]. On the basis of the sample voltage versus current dependences, the plot between lnJ against $F^{1/2}$ (Figure A.7) was plotted for I-V data‟s in the high field region. It is seen that ln J against $F^{1/2}$ shows linearity in the high field region, which indicates the either Poole-Frenkel or Schottky charge transfer mechanism takes place in this nanocomposite [43]. The HAP nanorod enhances the electrical properties of the graphene oxide layers and it can be a potential candidate for biosensor and catalytic applications.

References

1. O. Jost, A. Gorbunov, X. J. Liu, W. Pompe and J. Fink, J. Nanosci. Nanotechnol. 4 (2004) 433.
2. D. A. C. Brownson and C. E. Banks, Analyst, 135 (2010) 2768.
3. A. K. Geim and K. S. Novoselov, Nature Mater. 6 (2007) 183.
4. M. I. Katsnelson, Mater.Today, 10 (2007) 20.
5. Z. B. Jang and A. Zhamu, J. Mater. Sci. 43 (2008) 5092.
6. C. N. R. Rao, K. Biswas, K. S. Subrahmanyam and A. Govindaraj, J. Mater. Chem. 19 (2009) 2457.
7. H. Song, L.Zhang, C. He, Y. Qu, Y. Tian and Y.Lv, J. Mater. Chem. 21 (2011) 5972.
8. J. Guo, R.Wang, W.W.Tjiu, J.Panb, and T. Liua, J. Hazard. Mater. 63 (2012) 225.
9. J. C. Claussen, A. Kumar, D. B. Jaroch, M. H. Khawaja, A. B. Hibbard, D. M. Porterfield and T. S. Fisher, Adv. Funct. Mater. 22 (2012) 3399.
10. S. Murphy, L. Huang and P. V. Kamat, J. Phys. Chem. C, 117 (2013) 4740.
11. J. Cheng and J. Du, Cryst. Eng. Comm. 14 (2012) 397.
12. N. Li, M. Cao, Q. Wu and C. Hu, Cryst. Eng. Comm. 14 (2012) 428.
13. S. Srivastava, K. Jain, V. N. Singh, S. Singh, N. Vijayan, N. Dilawar, G. Gupta and T. D. Senguttuvan, Nanotechnology, 23 (2012) 205501.
14. Y. W. Hsu, T. K. Hsu, C. L. Suna, Y. T. Nien, N. W. Pu and M. D.Gere, Electrochim. Acta, 82 (2012) 152.
15. Y. Qian, F. Ye, J. Xu and Z.G. Le, Int. J. Electrochem. Sci, 7 (2012) 10063.
16. T. Zeng, X. l. Zhang, Y. Ma, H. Niua and Y. Cai, J. Mater. Chem. 22 (2012)18658.
17. W. Zhang, F. Liu, Q. Li, Q. Shou, J. Cheng, L. Zhang, B. J. Nelson and X. Zhang, Phys. Chem. Chem. Phys. 14 (2012) 16331.
18. Q. Tang, L. Wang, K. Zhu, Z. Shan and X. Qin, Mater. Lett. 100 (2013)127.
19. K. Moses, L. S. panchakarla, H. S. S. Matte, B. Govidarao and C. N. R. Rao, Ind. J. Chem. 50A (2011) 123
20. J. J. Shia, W. Hua, D. Zhao, T. T. He and J. J. Zhu, Sens. Actuators. B, 173 (2012) 239.
21. K.Yamashita, H. Owada, T .Umegaki and T. Kanazawa, Solid State Ionics, 40/41 (1990) 918.
22. T.Takahashi, S. Tanase and O. Yamamoto, Electrochim. Acta, 23 (1978) 369.

23. M. Nagai, T. Nishino and T. Saeki, Sens. Actuators, 15 (1998) 145.
24. K. Mori, S. Kanai, T. Hara, T. Mizugaki, K. Ebitani, K. Jitsukawa and K. Kaneda, Chem. Mater. 19 (2007) 1249.
25. M. P. Mahabole, R. C. Aiyer, C. V. Ramakrishna, B. Sreedhar and R. S. Khairnar, Bull.Mater. Sci. 28 (2005) 535.
26. M. Nagai, T. Saeki and T. Nishino, J. Am. Ceram. Soc. 73 (1990) 1456.
27. G. C. Petrucelli, E.Y. Kawachi, L.T. Kubota and C. A. Bertran, Anal. Commun. 33 (1996) 227.
28. B. Wang, J. J. Zhang, Z. Y. Pan, X. Q. Tao and H. S. Wang, Biosens. Bioelectron. 24 (2009) 1141.
29. D. C. Marcano, D.V. Kosynkin, J.M. Berlin, A. Sinitskii, Z. Sun, A. Slesarev, L. B. Alemany, W. Lu and J. M. Tour, ACS nano, 4 (2010) 4806.
30. H. K. Jeong, Y. P Lee, M. H. Park, K. H. An and I. J. Kim, J. Am. Chem. Soc.130 (2008) 1362.
31. C. C. Chien and K. T. Jeng, Mater. Chem. Phys. 99 (2006) 80.
32. J. J. Niu and J. N. Wang, Electrochim. Acta, 53 (2008) 8058.
33. F. Tuinstra and J.L. Koenig, J. Chem. Phys. 53 (1970) 1126.
34. Y. Z. Ji, P. X. Shen, Y. Song and X. G. Zhu, Mater. Sci. Eng. B, 176 (2011) 711.
35. C. Xu, X. Wang and W.J. Zhu, J. Phys. Chem. C, 112 (2008) 19841.
36. S. K. Novoselov, K. A. Geim, V. S. Morozov, D. Jiang, Y. Zhang, V. S. Dubonos, V. I. Grigorieva and A. A. Firsov, Science, 306 (2004) 666.
37. Z. Luo, Y. Lu, A. L. Somers and C. T. A. Johnson, J. Am. Chem. Soc. 131 (2009) 898.
38. X. Yang, X. Zhang, Y. Ma, H. Yi, Y. Wang and Y. Chen, J. Mater. Chem. 19 (2009) 2710.
39. V. D. Leff, L. Brandt and R. J. Heath, Langmuir, 12 (1996) 4723.
40. C. Basavaraja, W. J. Kim, P. X. Thinh and D. S. Huh, Bull. Korean Chem. Soc. 33 (2012) 449.
41. G. Eda, G. Fanchini and M. Fanchini, Nat. Nanotechnol. 3 (2008) 270.
42. C. A. Ferrari and J. Robertson, Philos. Trans. R. Soc. Lond., Ser. A: Math.Phys. Eng. Sci. 362 (2004) 2477.
43. D. Soundararajan, Y. Lim, M. P. Chun and K. H. Kim, Electron. Mater. Lett. 9 (2013) 177.

Nanoscience and
Nanotechnology Letters
Vol. 5, 1–6, 2013

Spin Relaxation of $Gd_2O_3/NiFe_2O_4$ Core–Shell Nanoparticles

A. Rajesh[1], Alo Dutta[2 *], K. Gurunathan[1], and T. P. Sinha[2]

[1]Department of Nanoscience and Technology, Alagappa University, Tamilnadu 630004, India
[2]Department of Physics, Bose Institute, 93/1, Acharya Prafulla Chandra Road, Kolkata 700009, India

Nickel ferrite encapsulated gadolinium oxide ($Gd_2O_3/NiFe_2O_4$ core–shell nanoparticles (NPs) has been synthesized by polyol method and analyzed by transmission electron microscope (TEM). The particle size is found to vary from 10 nm to 24 nm. The dynamics of magnetic moment has been studied with the help of temperature dependent electron paramagnetic resonance (EPR) spectroscopy. Peak-to-peak line width (H_{pp} and 'g' value of the EPR spectra are found to increase with the decrease of temperature. The sample has the lowest value of both these parameters at room temperature, which indicates that $Gd_2O_3/NiFe_2O_4$ shows minimum loss and is suitable for high frequency devices. Temperature dependence of line width shows the dominance of spin–spin relaxation in this system. Spin number estimated from EPR studies increases while the spin–spin relaxation time (T_2 decreases with decreasing temperature. The effect of temperature on the magnetic properties of the $Gd_2O_3/NiFe_2O_4$ core/shell NPs and the underlying mechanisms have been discussed.

Keywords: Core–Shell Nanoparticles, Polyol Method, HRTEM, Electron Paramagnetic Resonance.

1. INTRODUCTION

In recent years, science and technology have considerably developed and have created various nanomaterials such as nanoparticles,[1 2] nanotubes,[3 4] nanofilms,[5 6] graphene[7 8] and nanoporous materials.[9 10] Among them, the core–shell nanoparticles (NPs) with magnetic components have attracted much interest in recent years in both fundamental research[11 12] and practical applications.[13 14] In magnetic core–shell NPs, the novel properties of magnetic components can be combined with those of another active component to make bifunctional or even multifunctional NPs.[15] Many fundamental properties of these magnetic core–shell NPs are still not well understood. The blocking temperature of NPs with a magnetic core and a nonmagnetic shell is mainly determined by the size of the magnetic core.[16] The core–shell NPs having magnetic core and nonmagnetic shell have also been investigated for biological applications.[17] However, magnetic properties of the inverse structure, such as, NPs with a nonmagnetic core and a magnetic shell, have rarely been studied. In most of the cases, the synthesis of the particles is complicated and expensive. Here we report the synthesis and the properties of nonmagnetic/magnetic core/shell NPs consisting of nonmagnetic core of Gd_2O_3 which is encapsulated in magnetic shell of $NiFe_2O_4$. We employ polyol method as a cost effective and versatile synthesis method. These core/shell NPs can be used as contrast agent to improve the visualization of magnetic resonance imaging (MRI) which is a diagnostic technique widely employed due to its capability to distinguish between healthy and pathological tissues.

The use of contrast agent for MRI depends on the ability of the agent to shorten the relaxation times (T_1 and T_2) of water protons. Each distinct tissue type has unique relaxation rates ($1/T_1$ and $1/T_2$ and a proton density which affect tissue contrast and image interpretation.[18] Relaxation rates $1/T_1$ and $1/T_2$ measure the rate that molecular spins after being perturbed by the radio-frequency wave inside a magnet return back to their energy equilibrium states. T_1 is called spin–lattice relaxation time that is the time needed for spins and their environment (dubbed "lattice") to reach energy equilibrium. T_2 is called spin–spin relaxation time and it is time for spins themselves to reach equilibrium after radio frequency wave perturbation. In the core/shell of $Gd_2O_3/NiFe_2O_4$, gadolinium oxide can serve as positive contrast agent to reduce T_1 relaxation time resulting in a brighter signal, while magnetic $NiFe_2O_4$

* Author to whom correspondence should be addressed.

Acta Metall. Sin. (Engl. Lett.), 2014, 27(2), 253–258
DOI 10.1007/s40195-014-0056-0

Spin-Relaxation of NiO Encapsulated Gd_2O_3 Core–Shell Nanoparticles

A. Rajesh · M. Manivel Raja · K. Gurunathan

Received: 29 August 2013 / Revised: 27 November 2013 / Published online: 19 April 2014

Abstract Nickel oxide encapsulated gadolinium oxide (Gd_2O_3/NiO) core–shell nanoparticles (Nps) has been synthesized by polyol method and analyzed by transmission electron microscopy. The particle size is found to vary from 25 to 35 nm. Raman spectra show the gadolinium oxide core material peaks are found to be diminished by the mass effect of the NiO shell material. The dynamics of the magnetic moment has been studied with the help of temperature dependent electron paramagnetic resonance (EPR) spectroscopy. Peak-to-peak line width (DH_{pp}) value of the EPR spectra increases with decreasing temperature. Temperature dependence of line width shows the dominance of spin–lattice relaxation in these systems, and it can be used as T_1 contrast agent. Spin number estimated from EPR studies increases with the decrease of the temperature. The interfacial exchange coupling between the core and shell region is found to be existing at very low temperatures as determined by EPR studies in this non-magnetic/antiferromagnetic (NM/AFM) core/shell nanosystem. The effects of the temperature on the magnetic properties of the Gd_2O_3/NiO core/shell NPs and the underlying mechanism have been discussed.

KEY WORDS: Nanocomposite; Magnetic material; Raman spectroscopy; Electron paramagnetic resonance (EPR); Spin-relaxation

1 Introduction

In recent years, science and technology have considerably developed and have created various nanomaterials such as nanoparticles [1], nanotubes [2], nanofilms [3, 4], graphene [5] and nanoporous materials [6]. Among them, the core–shell nanoparticles (Nps) with magnetic components have attracted much interest in recent years both in fundamental research [7] and practical applications [8]. The core–shell Nps are also been widely investigated for biological applications example drug delivery, cell labelling and magnetic resonance imaging (MRI) etc. [9]. These core/shell Nps can be used as a contrast agent to improve the visualization of MRI images, which is a diagnostic technique widely employed due to its capability to distinguish healthy tissues from affected tissues. Core/shell Nps can enter the cells and they act as efficient contrasting agent due to its better spin–lattice relaxation time [10, 11].

The use of contrast agent for MRI depends on the ability of the agent to shorten the relaxation time (T_1 and T_2) of water's protons. Each distinct tissue type has unique relaxation rates ($1/T_1$ and $1/T_2$) and a proton density, which affects tissue contrast and image interpretation [12]. Relaxation rates $1/T_1$ and $1/T_2$ measure the rate that molecular spins after being perturbed by the radio-frequency wave inside a magnet return back to their energy

Available online at www.springerlink.com/journal/40195

A. Rajesh K. Gurunathan (&)
Department of Nanoscience and Technology, Science Block, Alagappa University, Karaikudi 630 004, India
e-mail: kgnathan27@rediffmail.com

M. Manivel Raja
Defence Metallurgical Research Laboratory, Kanchanbagh PO, Hyderabad 500 058, India

Article

Journal of
Nanoscience and Nanotechnology
Vol. 15, 1–6, 2015
www.aspbs.com/jnn

Dielectric Relaxation of $NiFe_2O_4/Gd_2O_3$ Core–Shell Nanoparticles

A. Rajesh[1], Alo Dutta[2], K. Gurunathan[1 *], and T. P. Sinha[2 *]

[1]Department of Nanoscience and Technology, Alagappa University, Karaikudi, Tamilnadu 630004, India
[2]Department of Physics, Bose Institute, 93/1, Acharya Prafulla Chandra Road, Kolkata 700009, India

Gd_2O_3 encapsulated $NiFe_2O_4$ core–shell nano-particles (CSNPs) have been synthesized by chemical route. The phase formation of the materials is confirmed by X-ray diffraction analysis. The average particle size is found to be 60 nm by transmission electron microscope. The band gap of $NiFe_2O_4/Gd_2O_3$ CSNPs is obtained by UV-visible absorption spectroscopy. The observed band gap of 4.38 eV lies in between the individual band gap of Gd_2O_3 and $NiFe_2O_4$. The frequency-dependent dielectric relaxation of the material is investigated in the temperature range from 303 K to 543 K. The temperature dependent relaxation times are found to obey Arrhenius law having activation energy of 0.3 eV. The Nyquist plots of impedance data are analyzed by the RC equivalent circuit having a constant phase element. The dielectric relaxation is modelled by Havriliak–Negami technique in the electric modulus formalism. The frequency dependent conductivity spectra follow the double power law.

Keywords: Core–Shell Nanoparticle, Dielectric Relaxation, ac Conductivity, Havriliak-Negami Model.

1. INTRODUCTION

The advances in new synthesis techniques make possible to synthesis various types of multi-functional nanomaterials such as nanoparticles,[1 2] nanotubes,[3] nanofilms,[4 5] nanoporous materials[6] etc. Among them, nano-particles having core–shell structure are the subject of the investigation in recent years and may be an interesting material for the technological applications.[7] They possess unique physical and chemical properties[8 9] which can be tuned by changing the chemical composition as well as the size of the core and shell.[10–13] The technological application of any material depends upon its dielectric properties. The polycrystalline ferrites are very good dielectric materials. Younas et al.[14] have investigated the dielectric properties of $NiFe_2O_4$ and observed a semiconducting to metallic transition at 358 K due to the transition from localized charge carrier $[Fe^{3+}\text{-}O^{2-}\text{-}Fe^{3+}]/[Ni^{2+}\text{-}O^{2-}\text{-}Ni^{2+}]$ linkage to delocalized charge carrier $[Fe^{3+}\text{-}Fe^{2+}]/[Ni^{2+}\text{-}Ni^{3+}]$ linkage. This may be possible because, in the process of preparation of ferrites, under slightly reduced conditions, the divalent iron formed in the body of the ferrite material leads to high conducting grains. When such materials are cooled in an oxygen atmosphere, it is possible to form layers of very low conductivity over its constituent grains. Almost all the ferrites in the polycrystalline form have relatively high conducting grains separated by low conducting layers, so that they behave as a homogeneous dielectric material.[15] Grain size effect and processing route in the synthesis of ferrites have been found to have relationship among power loss, low eddy current losses and better magnetic properties. Small grain size has given rise to the low power loss and this is attributed to unique uniformity and higher chemical homogeneity and grain uniformity in Mn–Zn ferrites.[16] Gadolinium oxide (Gd_2O_3 in its crystalline and amorphous phases has been of research interest as a replacement gate oxide material for silicon dioxide because of its high dielectric constant.[17] Nanocrystals (NCs) of Gd_2O_3 have been investigated for their applications as a magnetic contrast agents[18] and host materials in light emitting materials.[19]

In the present work, we have investigated the dielectric properties of Gd_2O_3 encapsulated $NiFe_2O_4$ core–shell nano-particles (CSNPs) because the crystal phase of the core material can be stabilized by the shell material to

* Authors to whom correspondence should be addressed.